

1 **Low ozone bubbles observed in the tropical tropopause**
2 **layer during the TC4 campaign in 2007.**

3

4 Petropavlovskikh I.^{1,2}, E. Ray^{1,2}, S. M. Davis^{1,2}, K. Rosenlof², G. Manney³, R. Shetter⁴,
5 S. Hall⁴, K. Ullmann⁴, L. Pfister⁵, J. Hair⁶, M. Fenn⁷, M. Avery⁶

6

7 ¹ Cooperative Institute for Research in Environmental Sciences, University of Colorado,
8 Boulder, CO 80305, USA

9 ² Earth Systems Research Laboratory, NOAA, Boulder, Colorado, USA

10 ³ Jet Propulsion Laboratory, California Institute of Technology, Pasadena, California,
11 USA,

12 also at New Mexico Institute of Mining and Technology, Socorro, NM, USA

13 ⁴ National Center for Atmospheric Research, ESSL, Atmospheric Chemistry Division,
14 Boulder, Colorado, USA

15 ⁵ NASA Ames Research Center, Moffett Field, California, USA

16 ⁶ NASA Langley Research Center, Hampton, Virginia, USA

17 ⁷ Science Systems and Applications, Inc., Hampton, VA, 23666, USA

18

19

20 _____

21 I. Petropavlovskikh, NOAA/ESRL/GMD

22 325 Broadway, Boulder, CO, USA, irina.petro@noaa.gov

23

24 **Abstract:**

25 In the summer of 2007 the NASA DC8 aircraft took part in the Tropical Composition,
26 Cloud and Climate Coupling (TC4) campaign based in San Jose, Costa Rica. During this
27 campaign, multiple in-situ and remote-sensing instruments aboard the aircraft measured
28 the atmospheric composition of the Tropical Tropopause Layer (TTL) in the equatorial
29 region around Central and South America. Partial ozone column measurements above the
30 aircraft were derived from the CCD Actinic Flux Spectrometer (CAFS) instrument and
31 column ozone profiles were derived from the Differential Absorption Lidar (DIAL)
32 instrument. During the July 17 flight off the Ecuadorian coast, these instruments detected
33 well-defined “bubbles” of anomalously low ozone concentration ($\sim < 75$ ppbv) above the
34 aircraft in the TTL. Backward trajectories from meteorological analyses and the aircraft
35 in situ measurements suggest that the ozone-depleted airmass came from deep convection
36 in the Equatorial Eastern Pacific and/or Panama Bight regions at least 5 days before
37 observation by the DC-8. Although the precise origin of the airmass can not be identified
38 with any degree of confidence, the coherence of this low-ozone airmass after such a long
39 period of time has implications for the chemical composition and mixing in the TTL.

40

41

42 **Introduction.**

43

44 One of the NASA science objectives is to continuously monitor natural and
45 anthropogenic variability of atmospheric composition in response to climate change.
46 Various satellite programs, including the A-train satellites, provide atmospheric data
47 necessary to meet this objective. While satellite data help with the global view of the
48 changing atmosphere, the quality of these measurements is assured by comparisons with
49 suborbital and ground-based measurements. Strong vertical gradients exist in the ozone
50 distribution near the tropical tropopause that are not well resolved by most satellite
51 measurements due to the coarse vertical resolution. Studies have shown that ozone
52 changes in the tropical lower stratosphere are important for determining the magnitude
53 and sign of the ozone radiative forcing [*IPCC*, 2001; *Ramaswamy et al.*, 2001].
54 Additionally, as noted in Gettelman et al. [2009], modeled tropopause height levels and
55 cold point temperatures are sensitive to the amount of ozone near the tropopause. The
56 photochemical lifetime of ozone in the tropical tropopause layer (TTL) is several months,
57 so transport is the primary cause of changes in ozone mixing ratios. Because the TTL
58 serves as the gateway for air entering the stratosphere, it is of interest to study processes
59 that impact the distribution of radiatively active gases in that region.

60 The Aura satellite has multiple instruments providing global column or profile
61 ozone information [*Schoeberl et al.*, 2006; *Schoeberl et al.*, 2008]. The Aura Validation
62 experiment (AVE) project mission was designed to provide correlative measurements
63 from NASA aircraft at a variety of locations covering the satellite's spatial and altitude
64 coverage [*Froidevaux*, 2001; *Newman*, 2001]. During the past Aura ozone validation
65 activities, including AVE, P-AVE, CR-AVE, TC-4, and ARCTAS, the UV actinic flux

66 was measured by the CAFS (CCD based Actinic Flux Spectroradiometer) instrument (R.
67 Shetter and S. Hall, NCAR) aboard the NASA WB-57 and DC-8 aircraft platforms. The
68 Absorption Lidar (DIAL) system (J. Hair, NASA/Langley) has been flown on the NASA
69 DC-8 in P-AVE and TC4 missions.

70 In the summer of 2007 the NASA DC8 aircraft took part in the Tropical
71 Composition, Clouds and Climate Coupling (TC4) campaign based in Costa Rica.
72 Multiple in-situ and remote-sensing instruments aboard the aircraft were flown to
73 measure atmospheric composition of the TTL. The layer was first defined by Highwood
74 and Hoskins [1998] and Folkins et al. [1999], and the definition was refined by
75 Fueglistaler et al. [2009]. It is a region in the tropics (~12-18 km) which is significantly
76 impacted by deep convection, and whose properties are transitional between the
77 troposphere and stratosphere. Questions still remain regarding the exact impact of
78 convection as well as the time scales for chemistry and transport that affect the
79 composition of the TTL.

80

81 **Measurements and data.**

82

83 The TC4 campaign was based out of San Jose, Costa Rica during July and August
84 2007. Measurements were coordinated between three aircraft, providing coverage of the
85 stratosphere (ER-2), upper troposphere (WB-57), and low to middle troposphere (DC-8).
86 In this study, we exclusively use measurements from the DC-8, as the flight of interest
87 did not have simultaneous measurements from the other two aircraft. The DC-8 aircraft
88 was equipped with both in-situ and remote-sensing instruments. Measurements of ozone,
89 aerosol, cloud, water vapor, and other trace gasses were taken from aboard the aircraft.

90 Figure 1 shows the combined picture of all flight tracks accomplished by the NASA DC-
91 8. The DC-8 sampled the atmosphere over a very large region near equatorial Central and
92 South America. However, the phenomena we discuss in this paper, a low-ozone bubble
93 near the coast of Ecuador, was the only one observed during the TC4 mission.

94 The integrated ozone column (DU) above the DC-8 aircraft is derived from the
95 CCD Actinic Flux Spectroradiometer CAFS measurements during each flight
96 [*Petropavlovskikh et al.*, 2007]. Also, a Differential Absorption Lidar (DIAL) system
97 provides continuous measurements of ozone number density, aerosol scattering and
98 depolarization distribution above and below the aircraft level [*Browell et al.*, 1998]. The
99 DIAL measured number concentration is converted to mixing ratio by using modeled
100 molecular density for the latitude and month. In situ ozone (FastOz, NASA Langley
101 Research Center [*Avery*, this issue]), CO (DACOM, NASA Langley Research Center
102 [*Sachse et al.*, 1987]), MHP (CIMS, Caltech [*Eisele and Tanner*, 1991; *Mauldin et al.*,
103 1998; *Mount et al.*, 1997]) measurements were made from aboard the NASA DC8.

104

105 Launches of ozone and water vapor sondes were coincident with most of the TC4
106 flights. The launches were done from Juan Santa Maria airport, Costa Rica, San Cristobal
107 of Galapagos Islands, Ecuador and from Las Tables, Panama (the last location is part of
108 the NATIVE campaign, P.I. A. Thompson). Ozone profiles are available from all three
109 sites as well as relative humidity from a standard operational radiosonde. Research
110 quality water vapor measurements from a frost point balloon were only taken at the Costa
111 Rica and Galapagos sites.

112

113 Below, we use GOES-12 satellite (located over the equator at 75° W) images from
114 the TC4 region for identification of deep convection, and for moisture and temperature
115 analysis. Both visible (Channel 1) and IR (channel 4 at 10.5 microns) images are used in
116 this study. Brightness temperatures (from Channel 4) below -35 C) are designated by
117 colors – 10 C for each color change (green is between -65 and -75 C). All images shown
118 here have been degraded to a 6 km resolution from the original 1 km visible and 4 km IR
119 data.

120 This study focuses on analysis of measurements taken during one DC-8 flight.
121 The flight was on July 17, 2007, and the track is shown in dark lavender on Figure 1 and
122 also overlaid on a visible satellite image in Figure 5 (a). In particular, we examine one
123 unusual ozone feature and hypothesize on its origins.

124

125 **NASA DC8 Observations**

126 A depleted ozone column above the DC-8 aircraft was detected by both DIAL and
127 CAFS near the Ecuador coast on July 17, 2007. The total ozone column was also
128 measured by the OMI instrument aboard the Aura satellite. The OMI surface tracks on
129 July 17 2009 (similar to location of MLS tracks in Figure 5) were located in close
130 proximity to the depleted ozone episode location. The OMI data were then interpolated to
131 the latitude of the DC-8 flight tracks. Figure 2 shows time series of CAFS ozone
132 columns (green) derived above the altitude of the DC-8 for July 17 2007 flight. In
133 addition, the co-located OMI-TOMS v2.2 data are shown as total ozone column above
134 the clouds (magenta) and ozone columns above the surface (blue). The depleted ozone
135 column above the DC8 aircraft is found at about 17 UT (vertical red line in Figure 2).
136 The extension of the CAFS-derived partial ozone column data (green) with ozone

137 climatology [*Bhartia*, 2002] estimated below the DC-8 altitude (orange) creates a total
138 ozone column dataset (black symbols) that matches a similar reduction in the OMI-
139 TOMS total ozone column time series (seen in both blue and magenta symbols). It
140 suggests that the reduction in OMI-TOMS total ozone column is entirely confined to the
141 altitudes above the aircraft.

142 This anomaly in the CAFS and OMI ozone column observations occurs at the
143 same time that the DIAL vertical profile data shows a bubble of depleted ozone between
144 14 and 16 km. Figure 3 shows the time altitude contour plot of the DIAL ozone mixing
145 ratio for the part of the flight between 16:00 and 17:20 UT. This portion of the flight was
146 flown at an altitude of 11.3 km (until about 17:00 UT when the aircraft turned and
147 descended to 10.3 km altitude). Note that FASTOZ data are shown as thin line at altitude
148 of the NASA DC-8 aircraft (it is also shown in Figure 4). The ozone anomaly between
149 14 and 16 km altitude is measured twice in this time series (centered around 16:53 UT on
150 the south bound leg, and again around 17:05 on a parallel track heading north 0.4 degrees
151 longitude farther to the west). The variation in ozone noted here is approximately a factor
152 of 2, from a high value in the 15 km region of ~ 0.125 ppmv (or 125 ppb) to a low value
153 of ~ 0.06 ppmv (60 ppb).

154 In-situ ozone measurements were collected by the FastOz instrument [*Avery*, this
155 issue] aboard the DC-8. During most of this flight an average 40 ppb of ozone mixing
156 ratio was measured while sampling inside the cloud and 63 ppb when out of cloud (as
157 determined by ozone correlations with the Counterflow Virtual Impactor data aboard DC-
158 8, [*Noone et al.*, 1988; *Twohy et al.*, 1997]). Figure 4 shows FastOz data during the
159 portion of the flight when the DIAL observed the low ozone events at 15 km altitude.
160 Note, the FASTOZ data are plotted at various aircraft altitudes: at 11.3 km from 16:00 to

161 17:02 UT, and at 10.3 km from 17:05 to 17:15 UT (the period of the DC-8 descent is
162 indicated by two solid vertical lines). An intermediate ozone concentration during the
163 flight near the Ecuador coast (marked by two vertical dashed lines between 16:42 and
164 16:55 UT) at 11.3 km altitude is in the range of 50 ppbv. The absence of large gradients
165 in the ozone mixing ratio suggests mixed air and not fresh convection. Therefore, it
166 implies that the depleted ozone at 15 km altitude is not related to the local convection that
167 would have altered the ozone mixing ratios at the 11.3 km flight level.

168 Two of the other chemicals measured aboard the NASA DC-8 are CO (Carbon
169 Monoxide) and MHP (Gas Phase Methyl Hydrogen Peroxide or CH_3OOH), which can be
170 used as indicators of vertical transport. Both CO and MHP have significant effects on
171 hydroxyl (OH) radicals in the atmosphere by reducing their abundance and increasing
172 tropospheric ozone concentration [*Andreae et al.*, 1988; *Crutzen and Andreae*, 1990].
173 Elevated CO and MHP concentrations in troposphere in the tropics can be a consequence
174 of biomass burning [*Lee et al.*, 1997; *Wennberg et al.*, 1998]. At the same time,
175 tropospheric ozone distribution in tropics is also altered through interactions of pollution
176 with large-scale circulation and deep convection [*Newell et al.*, 1997; *Thompson et al.*,
177 2003]. Therefore, these chemicals can be used as tracers for vertical transport.

178 Figure 4 shows CO mixing ratios remaining unchanged when sampled directly
179 below the depleted ozone features (low-ozone time period is indicated by the first two
180 vertical dashed lines). CO and ozone data were anti-correlated during most of the flight.

181 The lack of the elevated MHP concentrations in the upper troposphere prior to 17:05 UT,
182 while high concentration (~ 500 pptv) levels were measured near the surface (spiral
183 portion of the DC-8 flight between $\sim 17:20$ and $18:40$ UT, not shown), suggests that DC-8
184 sampled air mass at 11.3 km was different from the polluted marine boundary layer. The

185 period of the DC-8 flight between 17:05 and 17:10 is co-incident in time with the second
186 DIAL sampling of the low ozone feature (between the second solid vertical line and the
187 right edge of the plot). The period of decreased in-situ ozone with increased CO and
188 MHP occurs right after a short descent from 11.3 to 10.3 km (indicated by two solid
189 lines), which suggests possible convective influence at the DC-8 aircraft level. Since the
190 DC8 was at a lower altitude and different longitude for the second pass it likely
191 encountered different dynamical conditions. Although high clouds were seen in the nadir
192 looking DIAL aerosol channel (with cloud top heights just below 10 km) up to 16:42 UT
193 and after 17:05 UT, the satellite images near the time of the aircraft flight do not indicate
194 any deep convection reaching up to the 14-16 km levels (see the following section for
195 more discussion). The depleted ozone at the NASA DC-8 level appears to be a narrow
196 layer located above the cloud tops and just above a slight enhancement in the DIAL nadir
197 aerosol image (not shown). There seemed to be an intercept of the upper outer fringe of
198 this layer at 16:57 UT, whereas the aircraft was on the lower outer fringe when it leveled
199 out at 10.3 km at 17:05 UT. There could very likely be the influence of shallower
200 convection at the DC-8 levels, with the possibility of transport from the East (see the later
201 section on back trajectories), but that convection isn't getting up to the levels where the
202 depleted ozone is detected. Moreover, the DIAL data show a disconnect in vertical
203 distribution with increased ozone mixing ratios at 13 km (Figure 2). Therefore, the MHP
204 and CO observations at the NASA DC-8 aircraft flight level provide supporting evidence
205 that the depleted ozone is not related to local vertical transport.

206

207 **GOES data and NCEP analysis.**

208 The Aura satellite surface tracks are shown in Figure 5, where the HIRDLS (H),
209 TES (+), and MLS/OMI (M) instrument sampling tracks are plotted over the GOES-12
210 satellite IR image at 17:45 UT. Channel 4 is the traditional IR window channel that
211 "sees" to the ground except where there are clouds; it is centered at 10.5 microns
212 wavelength band. The colors on the plot are used to indicate the cloud system, where the
213 colder the cloud - the brighter the white color on the plot. Brightness temperatures below
214 -35C are designated by colors with -10C for each color change, such that the green is
215 between -65 and -75 C. Thus, areas of bright colors represent deep convection. The three
216 most prominent areas of deep convection are located over the Pacific coast of Mexico,
217 Panama and northern South America.

218 A combination of NCEP analysis and GOES images were used to create
219 convective influence plots for the area under question [*Pfister et al.*, 2001]. The back
220 trajectories were run for 8 days prior to the event on July 17, 2007, and were stopped
221 when found to be convectively influenced. The geo-location of the air parcels was
222 checked against the GOES images for bright clouds that are indicative of deep convection
223 events. Based on the DIAL ozone curtain plots, it appears that the depleted ozone area
224 ranges from about 14.9 (or ~49 kft) to 15.7 km (or ~52 kft) geometric altitude. Therefore,
225 the lower limit for trajectories was placed at a pressure of 134 mb, while the upper limit
226 was extended to 117 mb.

227

228 **Back Trajectory Analysis of the low-ozone air mass**

229

230 In this section, backwards trajectory calculations and satellite data are analyzed to
231 examine the evolution and identify the likely source region of the low-ozone airmass
232 observed from the DC-8 on the July 17 flight.

233 For the analysis presented here, 10-day back trajectory calculations were
234 performed using the HYbrid Single-Particle Lagrangian Integrated Trajectory
235 (HYSPLIT) model [Draxler, 1998; Draxler *et al.*, 1997; Draxler, 2003]. The input
236 meteorological data for HYSPLIT are from the NCEP Global Data Assimilation System
237 (GDAS, 1° x 1° resolution, <http://www.emc.ncep.noaa.gov/modelinfo/index.html>).
238 Isentropic back trajectories were initialized at 17 UT on 17 July 2007 over a matrix of 9
239 latitudes and 8 longitudes spanning the bounding latitude/longitude box of the region
240 over which the DC-8 observed the low-ozone bubble (near Ecuador coast, 3 degrees S
241 and 82 degrees W, between 16:30 UT and 17:00 UT). Additional model runs (not
242 shown) were performed using combinations of the GDAS omega vertical velocity as well
243 as different initialization times (16 Z and 18Z) to investigate the sensitivity of the results.
244 Although the endpoints of these runs differ slightly from the nominal run, the results
245 below are not sensitive to these small perturbations in initialization time or vertical
246 velocity assumptions. The trajectories were stopped whenever the convective influence
247 analyses (described in the previous section) suggested the intercept with the deep
248 convective system.

249 Figure 5 shows the nominal back trajectory runs initialized at the altitude of the
250 low-ozone bubble (15.4 km, top panel) and at the mean altitude of the DC-8 during the
251 low-ozone bubble measurement (10.4 km bottom panel).. The backward trajectory
252 analysis plots illustrate that the air-masses at the DC-8 altitude and 15 km are of
253 significantly different origin, with the flight-level air-mass originating from the East over

254 South America, and the 15 km air-mass originating from the West and ultimately
255 North/Northeast over the Panama Bight region.

256 The 15-km back trajectories were tracked backwards in time to the point at which they
257 intercepted convection, as defined by low brightness temperatures (< 238 K, or blue
258 colors in the figures shown here) in GOES Channel-4 imagery. As the trajectories make
259 their turn and head north, we find convective influence in the time range > 5 days old. All
260 trajectories intercepted convection between the 10 and 12 July, between 5 and 7 days
261 before being measured by the DC-8. The southernmost trajectories (black through light
262 blue colors) encountered convection in the Panama Bight and E. Pacific region, whereas
263 the northernmost trajectories encountered convection off of the East coast of Columbia,
264 over Columbia, and over Venezuela (green through red colors). Although the convective
265 source of the trajectories at a given initialization latitude is somewhat sensitive to the start
266 time and vertical velocity used (i.e., isentropic vs. omega), all of the combinations of
267 backward trajectories yield convective sources in the vicinity of Panama and Columbia.
268 Because the GOES brightness temperatures are consistently lower over Panama for the
269 trajectories considered here, we hypothesize that the low-ozone bubble airmass originated
270 over this region. Overall, these back trajectories support the idea that low-ozone air
271 detrained from deep convection over the South and Central America regions can be
272 transported through the TTL over long times (~ 7 days) and distances (~ 1000 km) in a
273 coherent manner (i.e., without significant mixing).

274

275 **Satellite observations.**

276 In support of our hypothesis of long-range transport from the Panama region, we
277 present data from the two coincident times over the course of the 10-day trajectories in

278 which the air parcels were located in the proximity of Aura/HIRDLS measurements
279 [*Gille et al.*, 2008]. The trajectory locations over GOES IR imagery are shown in (a)
280 panels of Figures 6 and 7, while the HIRDLS ozone data for these times are shown in (b)
281 panels of Figures 6 and 7.

282 The HIRDLS V4 ozone profile data covers a wider range of latitudes, while
283 profiles are about 100 km apart, so its resolution does not contain the fine horizontal
284 details observed by DIAL. However, the vertical resolution of HIRDLS is about 1 km,
285 which should be sufficient for identifying the vertical ozone gradient. The sequence of
286 two HIRDLS ozone pressure-latitude cross sections accompanied by the GOES IR
287 images and trajectories is shown in Figures 6 and 7. Figure 6 (a) shows the trajectory
288 locations on 16 July over the Eastern Pacific ocean, far from the regions of persistent
289 convection off the coasts of Central America. Also, a region of low-ozone air close in
290 space and time to the altitude of the back trajectories (~15.25 km) is present in the
291 HIRDLS data taken at ~21:20 UT (see panel (b) in Figure 6). Because of the lack of
292 convective clouds in this region of low ozone, as evidenced by the high brightness
293 temperatures in the GOES imagery, we hypothesize that this low-ozone region in the
294 HIRDLS data is the same airmass measured on 17 July by the DC-8. The region below
295 15 km where no data exist (white) may be due to the presence of clouds or where ozone
296 concentrations are below the HIRDLS detection limit [*Nardi et al.*, 2008].

297 Figure 7 (a) shows the trajectory locations at 21 UT on 10 July plotted over
298 GOES-12 IR image (upper panel), as well as data from the HIRDLS overpass at ~20:25
299 UT (lower panel). This time is within one day after the trajectories (purple and blue in
300 the figures) intercepted convection in the region. The HIRDLS data indicate a
301 widespread region of low-ozone air over Central America. Part of this data is associated

302 with convective clouds north of 10° along the HIRDLS track (i.e., the yellow dashed line
303 in Figure 7 (b)), whereas some of the data comes from regions free of convection at the
304 time of measurement. It is likely that this large region of low-ozone air seen from 5 –
305 15°N on 10 July contributed to the low-ozone air-mass observed on 17 July by the DC-8,
306 although a definitive attribution is not possible.

307 The above results support our hypothesis that the episodes of low ozone found in
308 the DC-8 measurements in the non convective region originate from long-range transport
309 of convectively-influenced, low-ozone air that has maintained some integrity for several
310 days. These results suggest that quasi-horizontal mixing processes in the Upper Tropical
311 Troposphere (UTT) are relatively slow. Deep convection over Panama is likely the
312 source of the observed low ozone “bubble”.

313

314 **RDF (reverse domain filling) analysis**

315 The BT analysis discussed above suggested the possibility of the long-range
316 adiabatic transport of the low concentration ozone “bubble” to the Ecuador coast from the
317 Panama region where it was generated by the deep-convection mechanism. The DIAL
318 and CAFS instruments detected a low ozone bubble between 14 and 16 km altitude
319 around 17 UT during the NASA DC-8 aircraft flight on June 17 2007. In this section we
320 attempt to validate our long-range transport hypothesis by using reverse domain filling
321 (RDF) calculations [*Sutton et al.*, 1994] [*Manney et al.*, 1998] driven by GEOS-5 data
322 assimilation system meteorological analyses [*Reinecker*, 2007].

323 The RDF analysis was used to infer the transport of ozone features noted here. In
324 the calculations, trajectory calculations using the GEOS-5 winds are started on a dense

325 grid (0.25 degrees latitude by 0.40 degrees longitude) and run back 8 days; at that time,
326 gridded MLS or HIRDLS data are interpolated to the parcel locations to provide an
327 estimate of the ozone that was transported to the starting locations of the trajectories.
328 Thus, the RDF maps/profiles from MLS/HIRDLS are based on transport by GEOS-5
329 winds and initialization with a single day of MLS or HIRDLS gridded data. Figure 8 (a)
330 shows the MLS initialized run, which looks consistent with the location of the DC-8
331 found low ozone bubbles near Ecuador on July 17 2007. Gradients comparable to those
332 observed from the DC-8 are seen in the RDF generated ozone field, indicating that
333 transport over 8 days can indeed generate features like those observed. The RDF
334 procedure was also applied to several other chemical species measured by MLS (H₂O,
335 CO and HNO₃, results are not shown), which show strong consistency in the morphology
336 of the RDF fields with those for ozone; this is evidence that the RDF calculations are
337 largely showing transport of real atmospheric features, since the "noise" (i.e., spurious
338 values) would not in general be expected to be correlated in all the species.

339 Results in Figure 8 (a) suggest that the low ozone feature in the RDF analysis near
340 the coast of Ecuador at the 360 K potential temperature level (near 15 km altitude, see
341 Figure 3) are similar to the DIAL-observed low ozone mixing ratios between 14 and 16
342 km altitude. The light blue colored filament of ozone that represents low ozone mixing
343 ratio of 50 ppbv extends to the west from the Ecuador coast (DC-8 tracks are marked by
344 white line) and then loops under the red-colored (higher mixing ratio) ozone feature in
345 the middle of the plot, and then extends to the north up to the Coast of Mexico. The
346 ozone feature may be smoothed out because of the initialization with MLS low resolution
347 ozone, but it is still indicative of the transport-related ozone residuals between 14 and 16
348 km altitude.

349 Results of an RDF analysis “transporting” equivalent latitude [*Butchart and*
350 *Remsberg, 1986*] are shown in Figure 8 (b). The equivalent latitudes are the latitudes that
351 would enclose the same area as the PV contours, thus showing at what equivalent latitude
352 the air at each point in the plot originated 8 days previously. The light sand colored
353 filaments seen near the south end of the DC-8 flight track (shown as white line) suggest
354 that the low ozone “bubble” most likely originated at about 10 degrees N. The RDF
355 analyses support our hypothesis of the origination of the low ozone “bubble” in the
356 InterTropical Convergence Zone (ITCZ) zone as the region of the deep convective
357 processes at low northern latitudes.

358

359 **Discussion and Conclusions**

360 The TTL is a region that is infrequently perturbed by convection [*Gettelman et*
361 *al., 2002*]. This allows ozone mixing ratios in the TTL to be significantly greater (red
362 color in DIAL data in Figure 3) than in the free tropical troposphere below 14 km, a
363 region heavily influenced by convective mixing as noted by the ozone gradients in the
364 DAIL data shown in Figure 3. A typical tropical ozone profile during the TC4 campaign
365 showed low ozone through the bulk of the troposphere (up to ~16 km, or the approximate
366 height of the tropopause), with a sharp gradient increasing to maximum values near 30
367 km. All the ozone measurements from the Panama site taken during TC4 are shown in
368 the Figure 9. There is significant variability near 15 km, not unlike the range noted in
369 the single DC-8 flight with the DIAL measurements. The temporal variation at Panama
370 is comparable to the spatial variation seen in the DIAL measurements, with minimums on
371 the order of 0.05 ppmv and maximums as high as 0.15 ppmv. Five of the Panama sondes
372 launched during TC4 show low values (below 0.07 ppmv) in the 14-16 km level, which is

373 ~20% of the time. This indicates that such phenomena are not an uncommon occurrence,
374 and hence likely contribute to the overall ozone budget in the UTT. Because of this, it is
375 of interest to study this particular case observed by the DC-8 in further detail.

376 One goal of the TC4 mission was to characterize the chemical boundary
377 conditions below the TTL, particularly for ozone. In the UTT the chemical lifetime of
378 ozone is about 50 days, and is much longer than the mixing time due to frequent
379 strenuous ITCZ related convection. In situ measurements from aircraft were analyzed to
380 characterize the statistical vertical distribution of ozone created by the convective
381 redistribution of ozone [Avery, this issue]. The statistics of ozone measured during the
382 mission between 7° S and 17° N and between 270° and 290° W shows that very fresh
383 convective outflow chemically more closely resembles in situ ozone sampled at about 3
384 km than it does at the surface, suggesting that vertical transport in the middle troposphere
385 is predominantly 3-10 km, and that entrainment/detrainment is more complicated than
386 just moving boundary layer air up to the tropopause.

387 The back trajectory analyses indicate that the low ozone features observed by
388 DIAL were the result of deep convective upwelling in the ITCZ, followed by roughly
389 isentropic transport to south of the equator. It is somewhat surprising that the low ozone
390 features were so pronounced after moving around the UT for a week or more, which may
391 reveal information on mixing time scales in the TTL. This is not inconsistent with results
392 recently published in James and Legras [2009], which show mixing times on the order of
393 a month in the subtropics above 350K.

394 One may question why this type of feature (unmixed low ozone) did not appear in
395 other DC-8 observations. As noted in Figure 1, very few flights ventured outside of the
396 convectively influenced region near the Panama bight. Hence, no distinct regions that

397 were convectively influenced would show up in the DIAL data (everything looks the
398 same). Such low ozone values in the TTL between 14 and 16 km are not completely rare;
399 low ozone values in the TTL were seen in DIAL data during the PEM-A and PEM-B
400 campaigns [Browell *et al.*, 2001; Browell *et al.*, 2003]. However, it should be noted that
401 the previous observations did not observe a similar spatially coherent low ozone "blobs"
402 seen during TC4. Because of the winds in this case, there is a contribution from
403 convection that is north of the equator and likely from the Panama region.

404 Some other points may be useful for further discussion. For example, the DIAL
405 ozone data on July 17 show large ozone values just below the ozone bubble, larger than
406 at similar altitudes on either side of the low-ozone area. It suggests the possibility of
407 some sort of exchange between the troposphere and stratosphere. However, on the other
408 hand the vertical and horizontal winds at the TTL levels were very slow, indicating that
409 this is also likely a horizontally transported feature.

410 There are other possibilities we have considered that could have caused the low
411 ozone features noted above 14 km on July 17th in the DIAL measurements. The DC-8
412 was flying in close proximity to the volcanic outflow from Ecuador. The chemical
413 reaction involving volcanic SO₂ → H₂SO₄ particles could be the reason for the ozone
414 destruction through the activation of chlorine. However, if that was the case, we would
415 expect to see aerosols present in the low ozone air mass. The contours in Figure 3 show
416 aerosols in the regions of elevated ozone in the 14-16 km levels, indicative of an aged air
417 mass, but there are no aerosols detected by DIAL in the low ozone bubble, hence
418 supporting the idea that it is a relatively "freshly" pumped up air mass.

419 Yet another mechanism of ozone destruction could be related to the combination
420 of high H₂O mixing ratios and occurrence of clouds below (apparent from backscatter in

421 DIAL aerosol backscatter data). It could lead to high photochemical destruction of ozone
422 through photochemical loss $J(\text{O}_3) \rightarrow \text{O}(^1\text{D}) + \text{H}_2\text{O} \rightarrow \text{OH}$, followed by additional ozone
423 loss through the HO_2/OH catalytic cycle. However, the DIAL/LASE system did not
424 detect high mixing water vapor above the DC-8 level, negating this as possible for this
425 case.

426 To summarize, based on the back trajectories (Figure 5 (a) coherent low ozone
427 bubble observed in the south part of the DC-8 flight of July 17, 2009 by the DIAL
428 instrument at ~17 UT between 14 and 16 km (green color in Figure 3) most likely
429 resulted from non local convection occurring in the Caribbean Sea, with possibly some
430 contribution from the Panama Gulf. Supporting evidence for the non locality and
431 subsequent transport comes from the fact that a low ozone region crossing the back
432 trajectories is seen in satellite observations in the absence of convection several days after
433 the convective event (Figure 6). There is also distinct difference in direction of
434 trajectories derived above aircraft level (Figure 5 (a)) and at aircraft level (Figure 5 (b),
435 South America), also supporting the non locality of the source. Therefore, ozone
436 depletion above the aircraft and elevated/reduced ozone mixing ratios at the aircraft level,
437 and increased ozone below the aircraft are governed by different processes. Further work
438 is needed to assess the magnitude of the contribution of convection to the ozone budget
439 of the tropospheric portion of the TTL.

440 **Acknowledgment**

441 This work was supported by the NASA Tropospheric Chemistry Program (M. Kurylo,
442 NASA HQ). The authors gratefully acknowledge helpful discussions with R .McPeters

443 (NASA/Goddard), K. Chance (Harvard), and E. Hilserath (NASA/HQ). We would also
444 like to emphasize the crucial contributions of the pilots and crew of the NASA DC-8
445 aircrafts. We would like to extend our gratitude to mission scientists (Brian Toon and
446 Dave Starr) and DC-8 platform scientists (Mark Schoeberl and Paul Wennberg) for
447 planning and successfully executing TC4 campaign. We greatly appreciate support from
448 the Aura HIRDLS team for providing us with the co-incident data and ozone curtain plots
449 (J. Gille and S. Karol of NCAR). All authors also would like to express endless thanks to
450 the support staff associated with the Aura Validation Experiment campaign that made the
451 CAFS measurements a success. Work at the Jet Propulsion Laboratory, California
452 Institute of Technology was done under contract with the National Aeronautics and Space
453 Administration. Special thanks are extended to Kurt Severance for help preparing the 3D
454 graphics.

455

456

457

458 **References**

459 Andreae, M. O., et al. (1988), Biomass-Burning Emissions and Associated Haze Layers
460 over Amazonia, *J Geophys Res-Atmos*, 93(D2), 1509-1527.

461 Avery, M. A., G. Diskin, G. Sachse, K. Severance, G. Morris, A. Thompson, C. Twohy,
462 E. Browell, J. Hair, M. Fenn, C. Butler, L. Froidevaux, G. Osterman, Ch. Trepte, R.
463 Salawitch, and T. Canty (this issue), Tropospheric Ozone Distribution by Convection in
464 the Central American ITCZ Region: Evidence from Observations of Ozone and Clouds
465 During the Tropical Composition, Cloud and Climate Coupling Experiment., *J Geophys*
466 *Res-Atmos*.

467 Bhartia, P. K. a. C. W. W. (2002), OMI TOMS-V8 Total O3 Algorithm edited by P. K.
468 Bhartia, pp. 15-31, NASA GSFC, Greenbelt, MD.

469 Browell, E. V., et al. (1998), Differential absorption lidar (DIAL) measurements from air
470 and space, *Applied Physics B-Lasers and Optics*, 67(4), 399-410.

471 Browell, E. V., et al. (2001), Large-scale air mass characteristics observed over the
472 remote tropical Pacific Ocean during March-April 1999: Results from PEM-Tropics B
473 field experiment, *J Geophys Res-Atmos*, 106(D23), 32481-32501.

474 Browell, E. V., et al. (2003), Large-scale ozone and aerosol distributions, air mass
475 characteristics, and ozone fluxes over the western Pacific Ocean in late winter/early
476 spring, *J Geophys Res-Atmos*, 108(D20), -.

477 Butchart, N., and E. E. Remsberg (1986), The Area of the Stratospheric Polar Vortex as a
478 Diagnostic for Tracer Transport on an Isentropic Surface, *J Atmos Sci*, 43(13), 1319-
479 1339.

480 Crutzen, P. J., and M. O. Andreae (1990), Biomass Burning in the Tropics - Impact on
481 Atmospheric Chemistry and Biogeochemical Cycles, *Science*, 250(4988), 1669-1678.

482 Darxler, R. R., Hess, G.D. (1998), An overview of the HYSPLIT_4 modelling system for
483 trajectories, dispersion and deposition, *Australian meteorological magazine*, 47(4), 295-
484 308.

485 Draxler, R. R., et al. (1997), *Description of the HYSPLIT_4 modeling system*, iii, 24 p.
486 pp., U.S. Dept. of Commerce, National Oceanic and Atmospheric Administration,
487 Environmental Research Laboratories, Air Resources Laboratory, Silver Spring, Md.

488 Draxler, R. R. a. R., G.D. (2003), HYSPLIT (HYbrid Single-Particle Lagrangian
489 Integrated Trajectory) Model edited, p. access via NOAA ARL READY Website, NOAA
490 Air Resources Laboratory, Silver Spring, MD.

491 Eisele, F. L., and D. J. Tanner (1991), Ion-Assisted Tropospheric Oh Measurements, *J*
492 *Geophys Res-Atmos*, 96(D5), 9295-9308.

493 Folkins, I., et al. (1999), A barrier to vertical mixing at 14 km in the tropics: Evidence
494 from ozonesondes and aircraft measurements, *J Geophys Res-Atmos*, 104(D18), 22095-
495 22102.

496 Froidevaux, L., and A. Douglass (2001), Earth Observing System (EOS) Aura Science
497 Data Validation Plan, Greenbelt, Maryland, 20771.

498 Fueglistaler, S., et al. (2009), Tropical Tropopause Layer, *Reviews of Geophysics*, 47, -.

499 Gettelman, A., et al. (2002), Distribution and influence of convection in the tropical
500 tropopause region, *J Geophys Res-Atmos*, 107(D10), -.

501 Gettelman, A., et al. (2009), The Tropical Tropopause Layer 1960-2100, *Atmos Chem*
502 *Phys*, 9(5), 1621-1637.

503 Gille, J., et al. (2008), High Resolution Dynamics Limb Sounder: Experiment overview,
504 recovery, and validation of initial temperature data, *J Geophys Res-Atmos*, 113(D16), -.

505 Highwood, E. J., and B. J. Hoskins (1998), The tropical tropopause (vol 124, pg 1579,
506 1998), *Quarterly Journal of the Royal Meteorological Society*, 124(551), 2536-2536.

507 IPCC (2001), *Climate Change 2001: The Scientific Basis. Contribution of Working*
508 *Group I to the Third Assessment Report of the Intergovernmental Panel on Climate*
509 *Change*, 994 pp.

510 James, R., and B. Legras (2009), Mixing processes and exchanges in the tropical and the
511 subtropical UT/LS, *Atmos Chem Phys*, 9(1), 25-38.

512 Lee, M., et al. (1997), Hydrogen peroxide, organic hydroperoxide, and formaldehyde as
513 primary pollutants from biomass burning, *J Geophys Res-Atmos*, 102(D1), 1301-1309.

514 Manney, G. L., et al. (1998), The 4-day wave and transport of UARS tracers in the austral
515 polar vortex, *J Atmos Sci*, 55(23), 3456-3470.

516 Mauldin, R. L., et al. (1998), A new chemical ionization mass spectrometer technique for
517 the fast measurement of gas phase nitric acid in the atmosphere, *J Geophys Res-Atmos*,
518 103(D3), 3361-3367.

519 Mount, G. H., et al. (1997), An intercomparison of spectroscopic laser long-path and ion-
520 assisted in situ measurements of hydroxyl concentrations during the Tropospheric OH
521 Photochemistry Experiment, fall 1993, *J Geophys Res-Atmos*, 102(D5), 6437-6455.

522 Nardi, B., et al. (2008), Initial validation of ozone measurements from the High
523 Resolution Dynamics Limb Sounder, *J Geophys Res-Atmos*, 113(D16), -.

524 Newell, R. E., et al. (1997), Western Pacific tropospheric ozone and potential vorticity:
525 Implications for Asian pollution, *Geophys Res Lett*, 24(22), 2733-2736.

526 Newman, P., R. Friedl, D. Fahey, and M. Ross (2001), Aura Validation Experiment
527 (AVE) White paper (version 1.0), Greenbelt, MD.

528 Noone, K. J., et al. (1988), Design and Calibration of a Counterflow Virtual Impactor for
529 Sampling of Atmospheric Fog and Cloud Droplets, *Aerosol Sci Tech*, 8(3), 235-244.

530 Petropavlovskikh, I., et al. (2007), Algorithm for the charge-coupled-device scanning
531 actinic flux spectroradiometer ozone retrieval in support of the Aura satellite validation,
532 *Journal of Applied Remote Sensing*, 1, -.

533 Pfister, L., et al. (2001), Aircraft observations of thin cirrus clouds near the tropical
534 tropopause, *J Geophys Res-Atmos*, 106(D9), 9765-9786.

535 Ramaswamy, V., et al. (2001), Stratospheric temperature trends: Observations and model
536 simulations, *Reviews of Geophysics*, 39(1), 71-122.

537 Reinecker, M. M. (2007), The GEOS-5 data assimilation system: A documentation of
538 GEOS-5.0, NASA.

539 Sachse, G. W., et al. (1987), Fast-Response, High-Precision Carbon-Monoxide Sensor
540 Using a Tunable Diode-Laser Absorption Technique, *J Geophys Res-Atmos*, 92(D2),
541 2071-2081.

542 Schoeberl, M. R., et al. (2006), Overview of the EOS Aura Mission, *Ieee T Geosci*
543 *Remote*, 44(5), 1066-1074.

544 Schoeberl, M. R., et al. (2008), Introduction to special section on Aura Validation, *J*
545 *Geophys Res-Atmos*, 113(D15), -.

546 Sutton, L. N., et al. (1994), High-Resolution H-1-Magnetic Resonance Spectroscopy of
547 Pediatric Posterior-Fossa Tumors in-Vitro, *Journal of Neurosurgery*, 81(3), 443-448.

548 Thompson, A. M., et al. (2003), Southern Hemisphere Additional Ozonesondes
549 (SHADOZ) 1998-2000 tropical ozone climatology - 2. Tropospheric variability and the
550 zonal wave-one, *J Geophys Res-Atmos*, 108(D2), -.

551 Twohy, C. H., et al. (1997), Measurement of condensed water content in liquid and ice
552 clouds using an airborne counterflow virtual impactor, *Journal of Atmospheric and*
553 *Oceanic Technology*, 14(1), 197-202.

554 Wennberg, P. O., et al. (1998), Hydrogen radicals, nitrogen radicals, and the production
555 of O-3 in the upper troposphere, *Science*, 279(5347), 49-53.

556

557

558

559 **Figures**

560

561 **Figure 1.** Composite of DC-8 tracks during the TC4 campaign in July-August of 2007
562 (courtesy of the NASA Langley DIAL team).

563

564 **Figure 2.** Ozone column data time series are shown for NASA DC-8 flight on July 17
565 2007. The co-incident OMI-TOMS v2.2 total ozone column data above the clouds
566 (magenta) and above the surface (blue) are plotted for comparisons with the combined
567 CAFS total ozone column (black): a combination of the CAFS-derived ozone column
568 above (green) and climatological ozone column below the NASA DC-8 aircraft level
569 (orange, offset by 150 DU). The approximate time of the low ozone value encounter (at
570 17 UT) is marked by red vertical line. The dashed vertical line marks the Aura satellite
571 overpass time at 19:30 UT.

572

573 **Figure 3.** Ozone mixing ratio profiles (ppbv) as derived by the DIAL instrument on
574 board the NASA DC-8 flight on July 17, 2007 are plotted as function of altitude and time.
575 The colors indicate different levels of ozone. The depleted ozone layer between ~14 and
576 16 km is marked with black oval. The corresponding latitude and longitude coordinates
577 of the DC-8 platform are also provided at the bottom of the plot. The aerosol contours are
578 plotted (white lines) over the ozone field to show the co-incident aerosol scattering
579 measurements.

580

581 **Figure 4.** In situ ozone (FastOz), carbon dioxide (CO, DACOM) and MHP (Gas Phase
582 Methyl Hydrogen Peroxide, CIMS) mixing ratios are shown at the aircraft level for
583 portion of the NASA DC-8 flight on July 17 2009. The time period between 16:45 and
584 16:55 UT (marked by two dashed vertical black lines) is co-incident with the DIAL low
585 ozone measurements at 14-16 km altitude range. The descent of the DC-8 from 11.3 to
586 10.3 km is pointed out by the two vertical solid black lines. The period of the DC-8 flight
587 between 17:05 and 17:10 is co-incident with the second DIAL sampling of the low ozone
588 feature. The decreased ozone, elevated CO and MHP levels suggest possible deep
589 convection influence.

590

591 **Figure 5. (a)** Backward trajectories initialized at the altitude and latitude/longitude of the
592 low-ozone air-mass (~15 km) are plotted over the GOES Channel 4 brightness
593 temperature imagery taken at 17:45 UT (colors from black to red indicate the starting
594 latitude of the trajectory, and diamonds are plotted at 00:00 UT on each day of the
595 trajectories). The DC-8 flight track is shown in white. **(b)** Same as **(a)**, but for
596 trajectories initialized at the DC-8 altitude (~ 10 km).

597

598 **Figure 6. (a)** GOES channel 4 imagery with back trajectory locations ending at 22 Z (+
599 signs) on 16 July, with HIRDLS measurement track plotted (H's and dashed yellow line).
600 **(b)** HIRDLS data, with yellow dashed line corresponding to location in top figure, and
601 plotted at the mean altitude of the back trajectories at the time of HIRDLS overpass
602 (21:20 UT). Black dashed line is the HIRDLS cloud-top altitude.

603

604 **Figure 7. (a)** GOES channel 4 imagery with back trajectory locations ending at 21 Z (+
605 signs) on 10 July, with HIRDLS measurement track plotted (H's and dashed yellow line).
606 **(b)** HIRDLS data, with yellow dashed line corresponding to location in top figure, and
607 plotted at the mean altitude of the back trajectories at the time of HIRDLS overpass
608 (20:25). Black dashed line is the HIRDLS cloud-top altitude.

609

610 **Figure 8. (a)** The latitude/longitude cross-section of the 8-day RDF analysis of the
611 GEOS-5 isentropically advected ozone mixing ratios at 360 K level. The MLS ozone
612 field was used to initiate RDF analysis. The DC-8 flight tracks are shown as white lines
613 in the middle of the plot. **(b)** The same as **(a)**, but for equivalent latitude data.

614

615 **Figure 9.** Ozone sounding mixing ratio measurements are plotted as function of time and
616 altitude. Las Tablas, Panama, NATIVE campaign (7.75 N, 80.25 W).

617

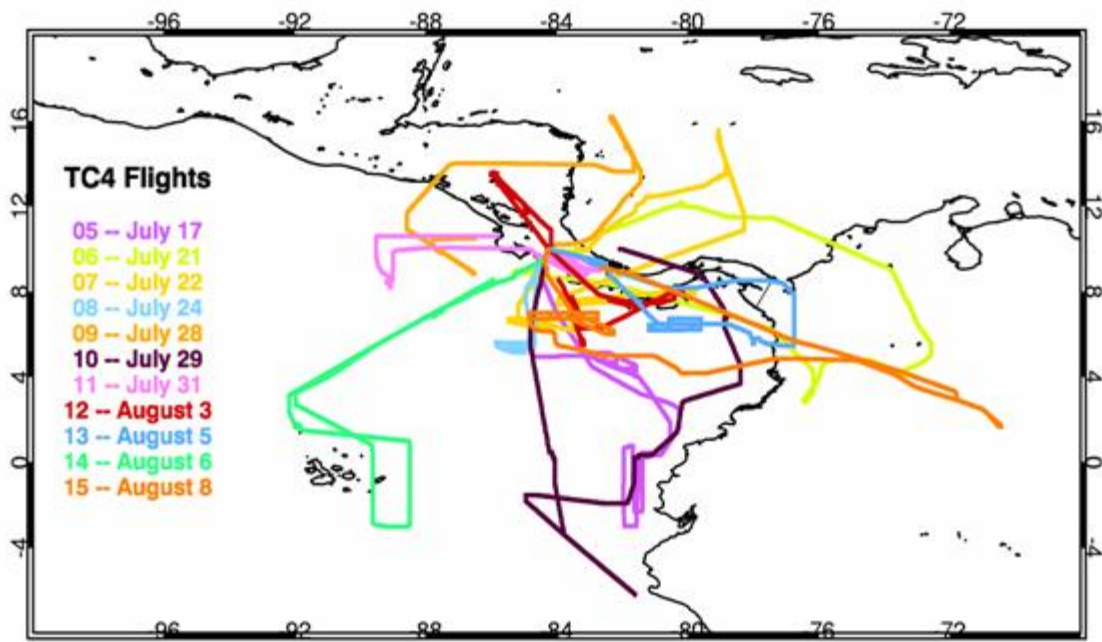
618

619

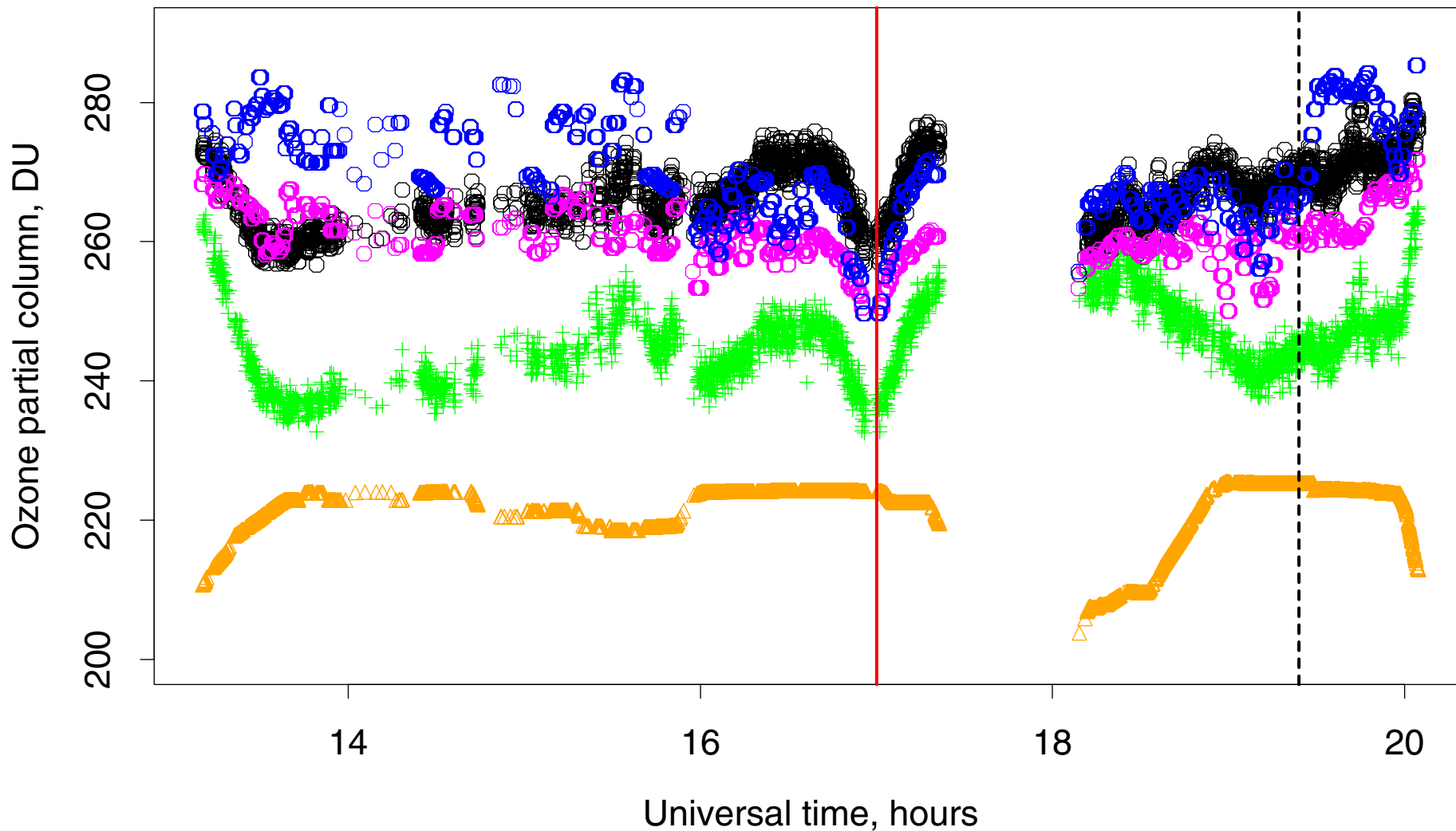
620

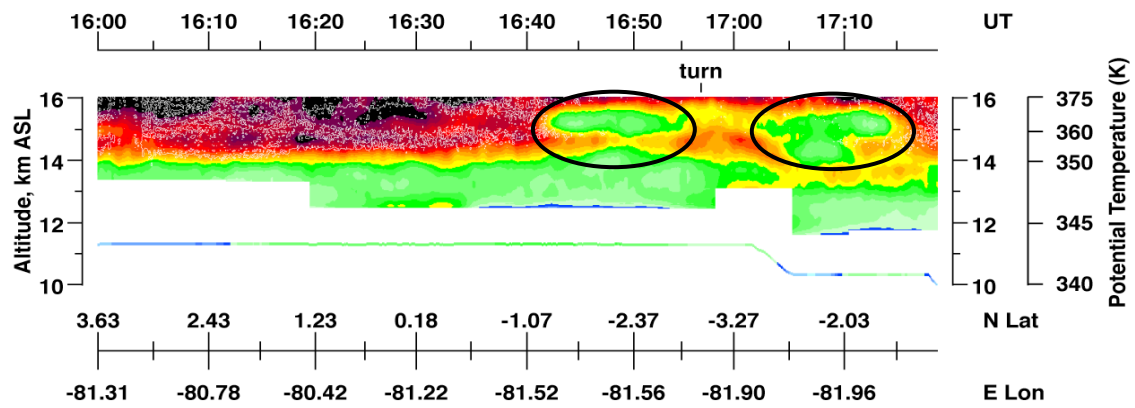
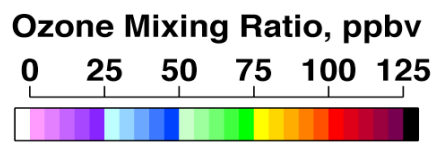
621

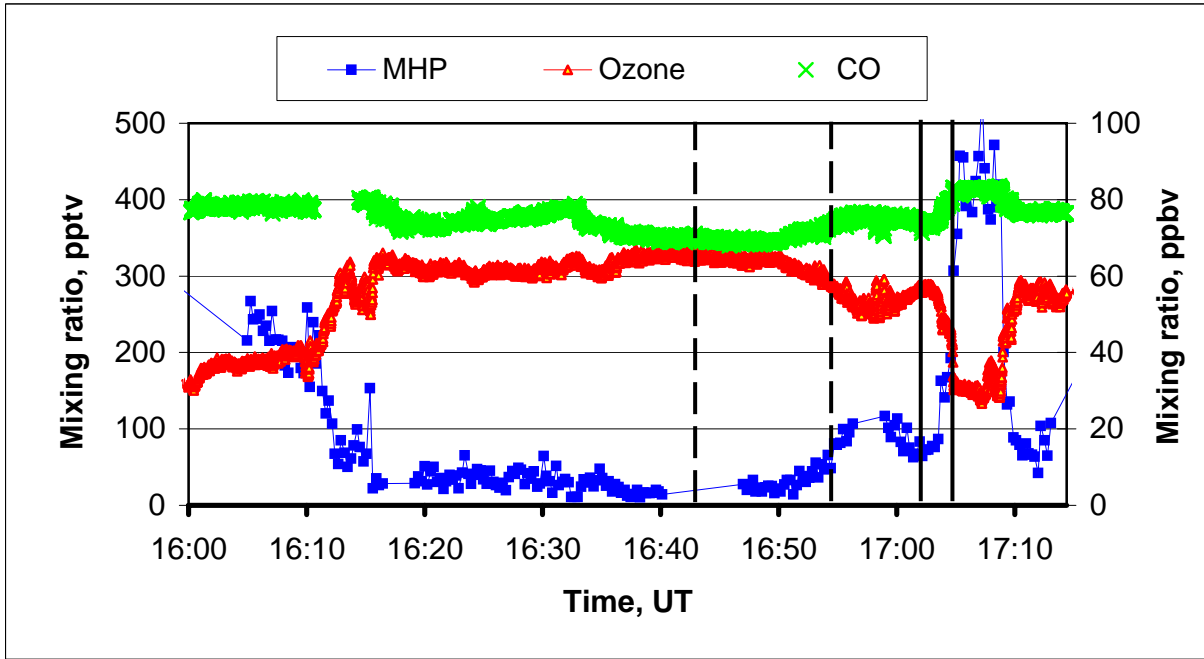
DC-8 Composite Flight Tracks
TC4: July 17 - August 8, 2007



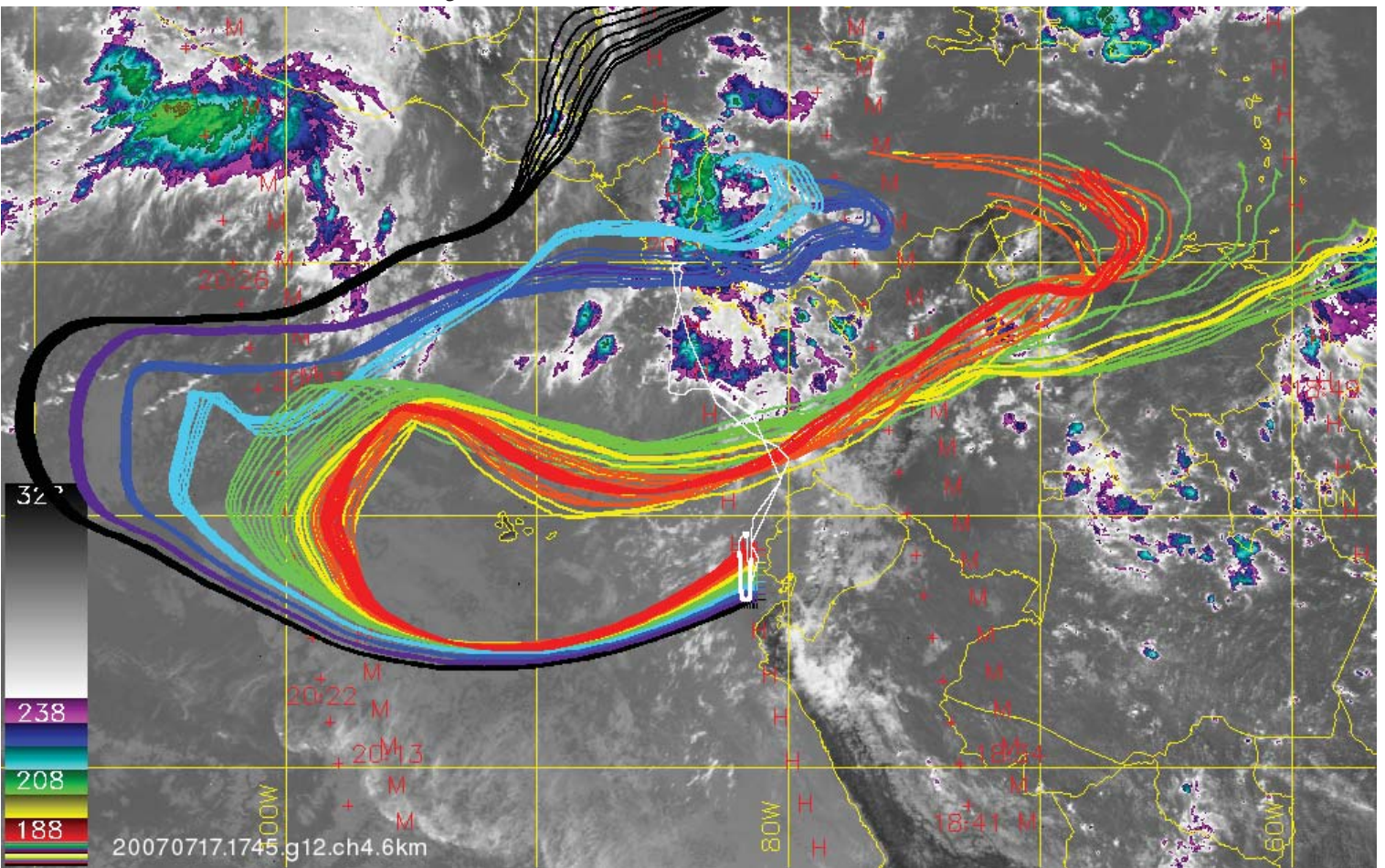
- OMI above cloud
 - OMI above and below cloud
 - +
 - △
 -
- CAFS ozone above aircraft
Climatology+200 DU
CAFS+Climatology



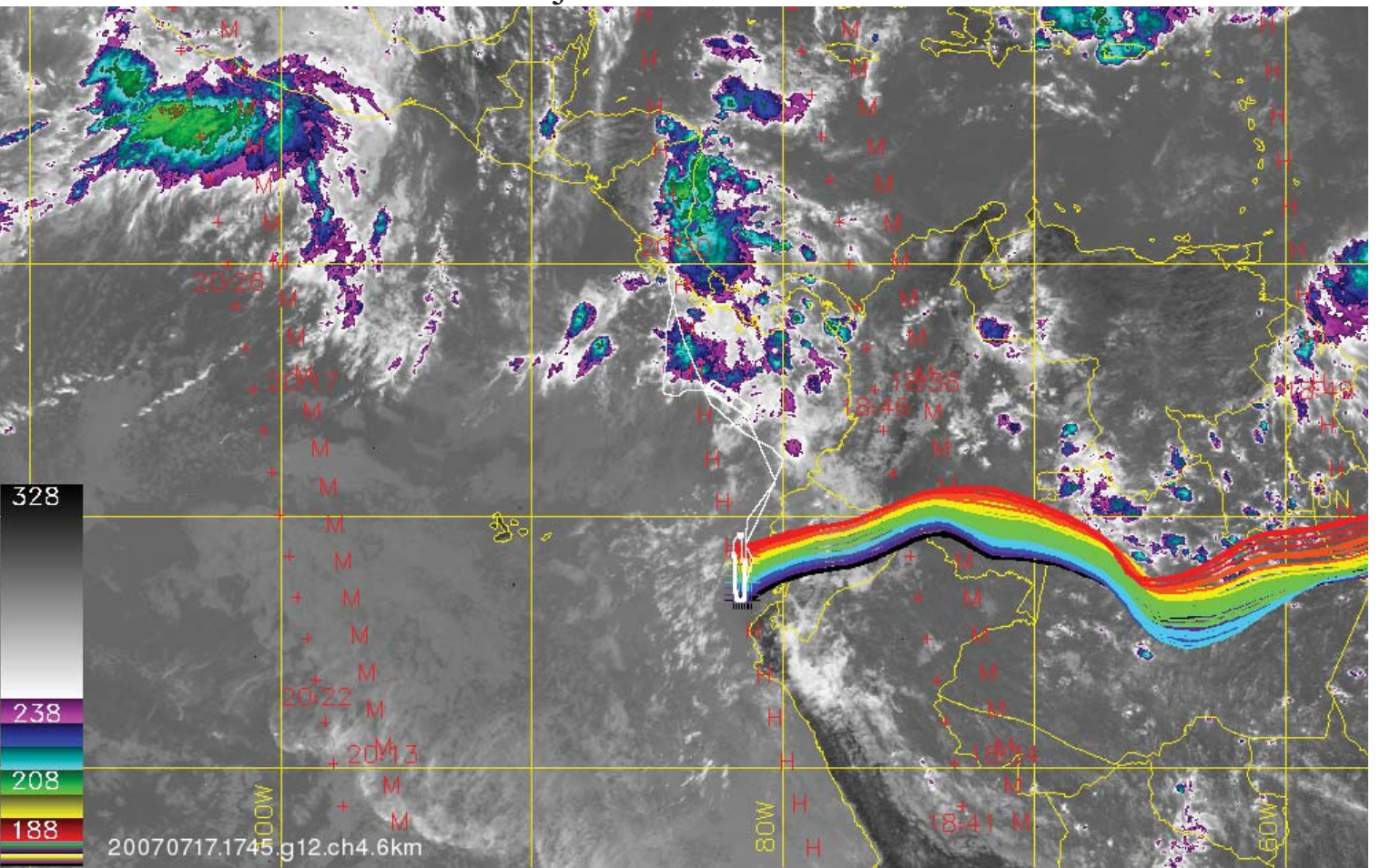


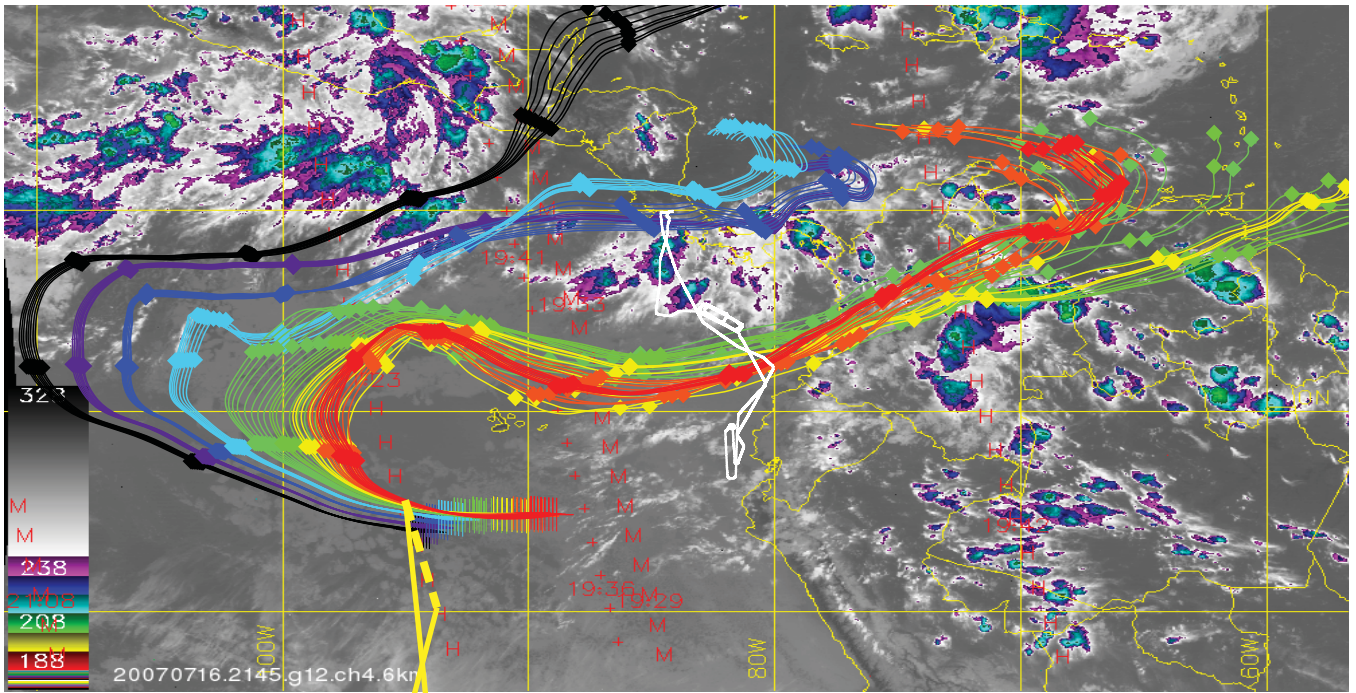


Backward trajectories at low-ozone bubble altitude

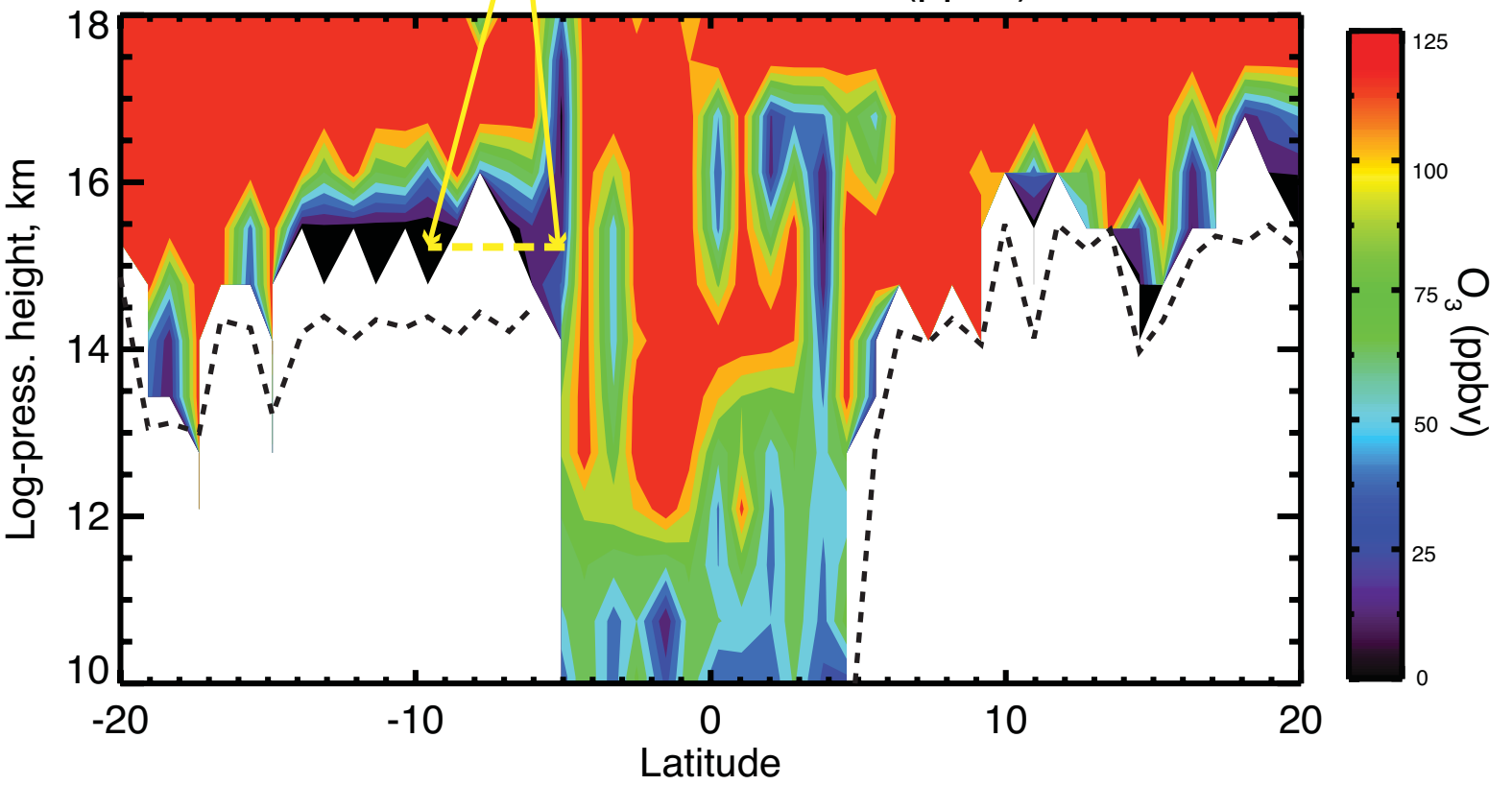


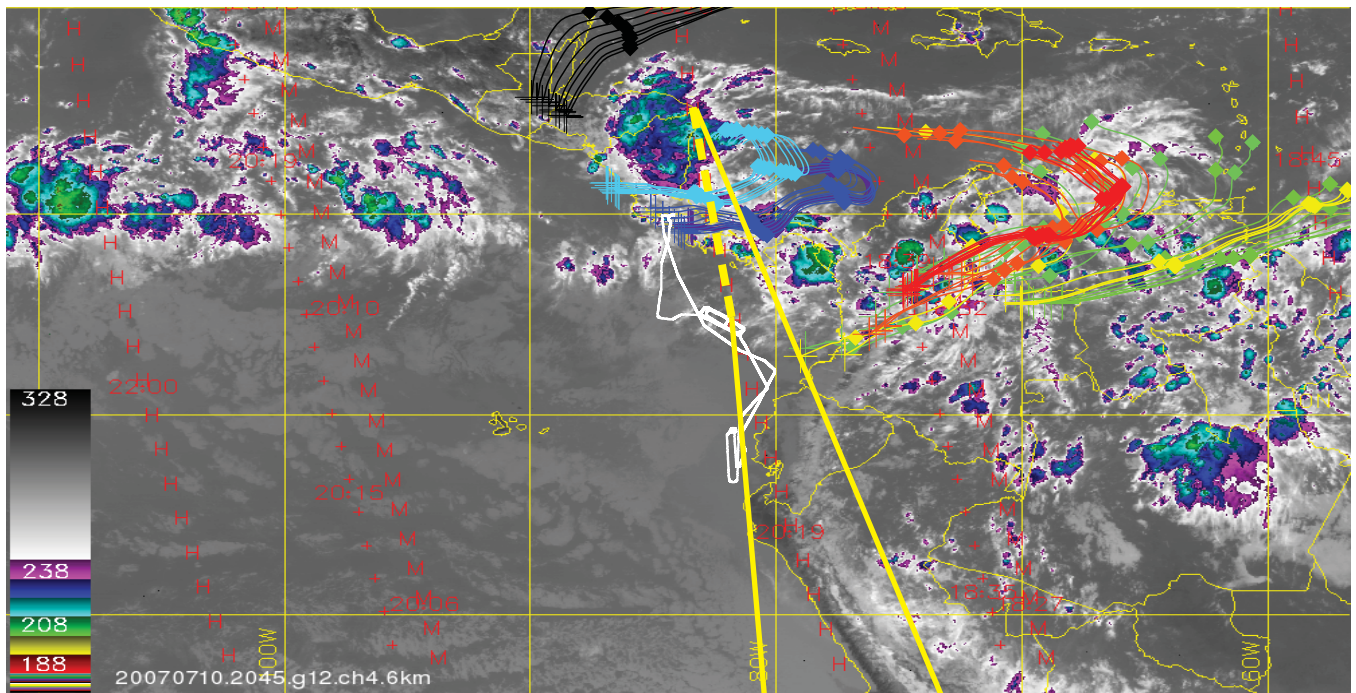
Backward trajectories at DC-8 altitude



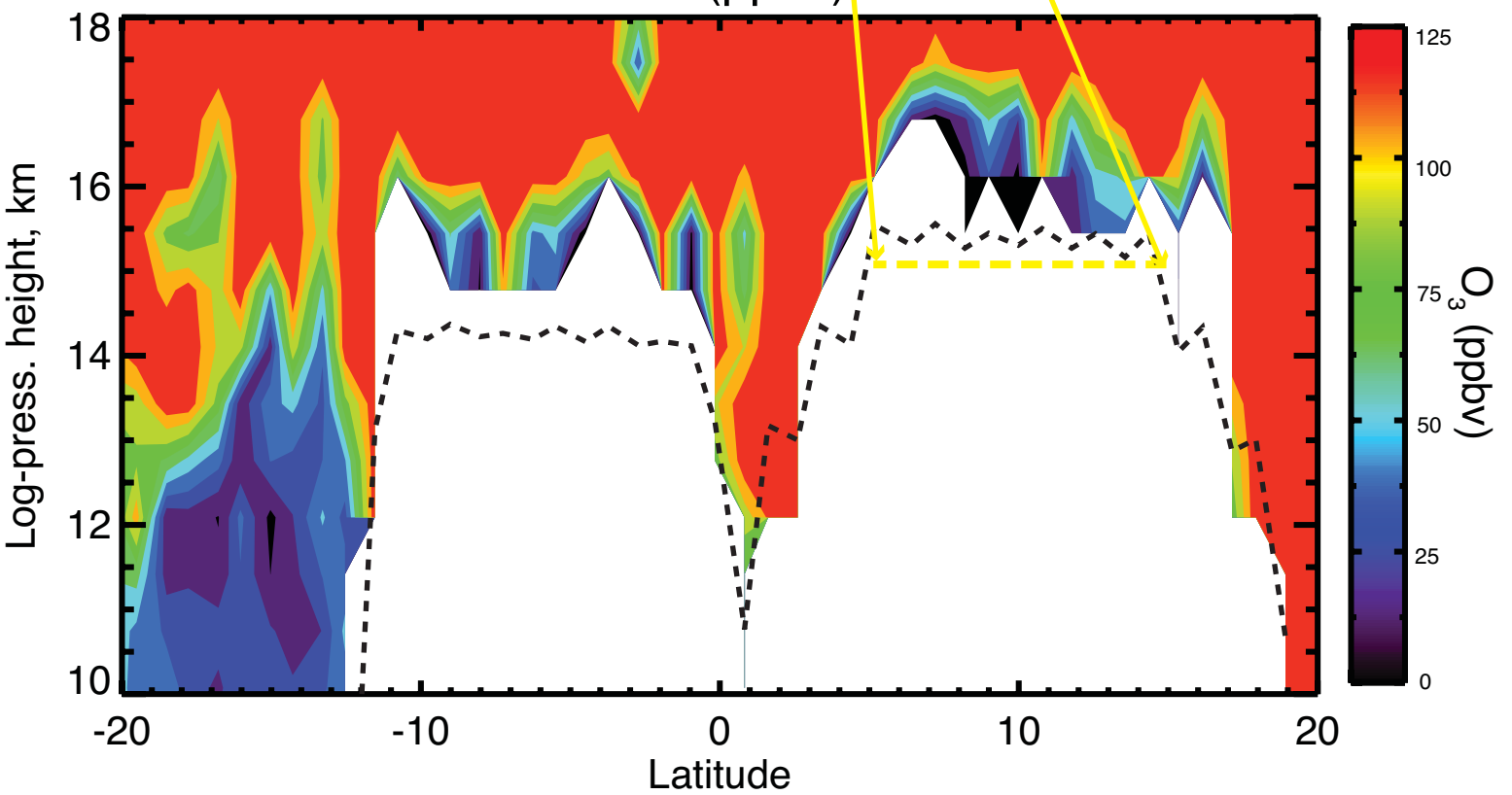


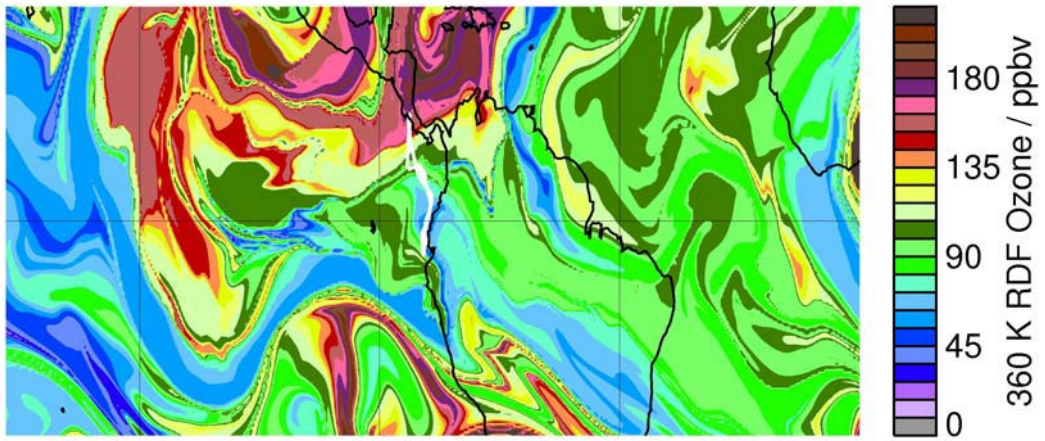
HIRDLS Ozone (ppbv)



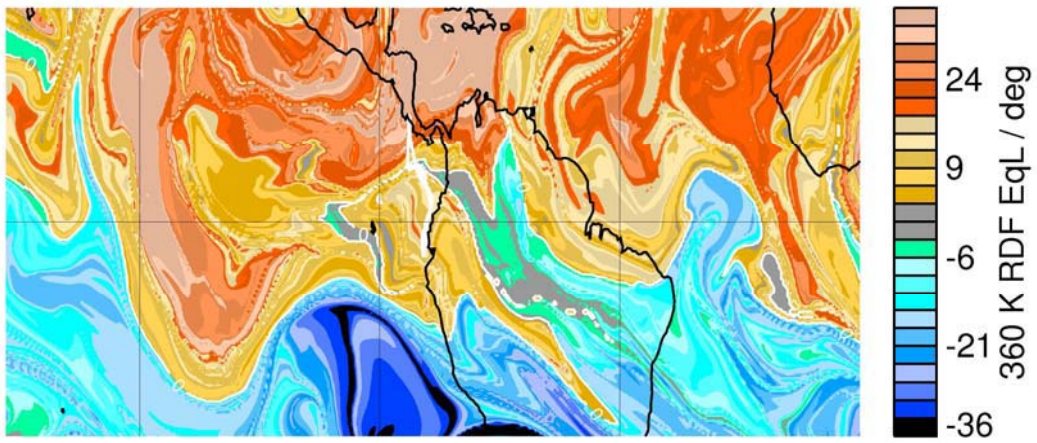


HIRDLS Ozone (ppbv)





(a)



(b)

Sondes at Native Trailer

